ELSEVIER

Contents lists available at ScienceDirect

Icarus

journal homepage: www.elsevier.com/locate/icarus



Check for updates

Aeolian driven silicate comminution unlikely to be responsible for the rapid loss of martian methane

Graham Purvis ^a, Emmal Safi ^b, John Edgar ^a, Corinne Wills ^a, Casey Dixon ^a, Lidija Šiller ^c, Jon Telling ^{a,*}

- ^a School of Natural and Environmental Sciences, Newcastle University, Newcastle upon Tyne, Tyne & Wear NE1 7RU, UK
- ^b National Physical Laboratory, Hampton Road, Teddington, Middlesex TW11 OLW, UK
- ^c NEXUS, School of Engineering, Newcastle University, Newcastle upon Tyne NE1 7RU, UK

ARTICLE INFO

Keywords:
Aeolian processes
Mars
Atmosphere
Nuclear magnetic resonance
Mineralogy
Methane

ABSTRACT

Seasonally varying levels of methane have been measured at parts per billion by volume levels in the lower Martian atmosphere. The source of this methane is not understood, but equally intriguing is its rapid loss, which is higher than the current chemical or photochemical decomposition models suggest. This implies an unknown but efficient sink mechanism. Earlier investigations reported the formation of Si• during the comminution of borosilicate glass and quartz that permitted the uptake of methane. This led to the speculation that an analogous aeolian driven comminution of Si-rich minerals on Mars could similarly sequestrate atmospheric methane. However, borosilicate glass is an artificial material and crystalline quartz is not common on the surface of Mars. To investigate whether this mechanism could take place on materials that were more representative of those on Mars, we comminuted a set of Mars analogue silicate rocks/minerals (basalt, obsidian, feldspar, pyroxene, zeolite, opal) in the presence of ¹³C-labeled methane. Solid-state Nuclear Magnetic Resonance (NMR) analysis of borosilicate glass and quartz indicated silicon carbide bond formation and this observation was supported by attenuated total reflectance-Fourier transform infra-red spectroscopy and X-ray photoelectron spectroscopy. However, silicon carbide bonds and methane sequestration were not detected in our set of Mars analogue samples. We hypothesise that electron donation by redox-active elements within the analogue materials, such as Fe, may have suppressed Si-methyl bond formation during comminution. Aeolian driven Si radical formation appears unlikely to be responsible for the rapid loss of methane in the Martian atmosphere, and thus the methane sink mechanism(s) require further investigation.

1. Introduction

The methane in the atmosphere of Mars could potentially serve as a biosignature of fossil or extant life (Lefèvre, 2019; Summers et al., 2002). Consequently, the remote detection of seasonally variable levels of methane at ppbv concentrations in the Martian atmosphere raised the intriguing possibility that this could be the first evidence for life outside the Earth (Formisano et al., 2004; Krasnopolsky et al., 2004). Additionally, it can provide insights into subsurface geochemical processes, such as water-rock reactions and the decomposition of clathrates or ancient accumulated meteoritic organics that could provide clues to the habitability of early or contemporary Mars (Franz et al., 2020; Oehler and Etiope, 2017). Those remote observations were more recently supported by measurements by the Mars Express Orbiter (Giuranna et al.,

2019) and in situ by the Curiosity Mars Science Laboratory (MSL; Webster et al., 2013). The Curiosity rover has detected average background methane levels of 0.24 to 0.65 parts per billion by volume (ppbv) with reports of levels spiking to $15.5 \pm 2.5 \, \text{ppbv}$ (Webster et al., 2015; Giuranna et al., 2019). Furthermore, a three-year analytical campaign by the Curiosity rover indicated that the methane levels appeared to exhibit cyclical seasonal variations with an average variation of 0.41 ppbv (Webster et al., 2018). The evidence of episodic emissions of methane on Mars of perhaps as much as 19 Kts at a time (Moores et al., 2019; Mumma et al., 2009) has been interpreted as indicating adsorption-mediated reactions, although the sources remain unknown. In contrast, however, the ExoMars Trace Gas Orbiter did not detect any methane providing instead an upper limit of <50 parts per trillion by volume (pptv) on the methane levels in the atmosphere 5 km above the

E-mail address: jon.telling@newcastle.ac.uk (J. Telling).

 $^{^{\}ast}$ Corresponding author.

surface, and <12 pptv in the northern latitudes above 3 km, perhaps suggesting that any fluxes of methane to the atmosphere are highly localised in space and/or time (Korablev et al., 2019).

Mechanisms for losses of methane from the Martian atmosphere are equally enigmatic. Photochemical modelling has suggested that the methane in the Martian atmosphere should degrade between 250 and 670 terrestrial years (Formisano et al., 2004; Krasnopolsky et al., 2004; Lefèvre and Forget, 2009; Summers et al., 2002; Wong et al., 2003). However, the observed residence time of methane in the Martian atmosphere has been estimated to be ca. 0.4 to 4 Earth years (Lefèvre and Forget, 2009; Mumma et al., 2009). Therefore, an efficient but unidentified sink mechanism appears to be responsible for a ca. 75-850 fold increase in the rate of methane loss. The sequestration of methane through biological activity appears to be unlikely, as calculations suggest that the ppbv methane levels detected would impose a severe kinetic limitation on the gain of cellular energy for any hypothetical methanotrophic organisms (Seto et al., 2019). Thus, an interaction between the Martian atmosphere and the geosphere would be a more plausible sink mechanism.

Aeolian activity is the dominant weathering process for erosion and mineral transport on Mars (Greeley et al., 1982). The dust lifted into dust devils and storms can induce strong electrical fields, which may enhance the production of $\rm H_2O_2$ or other super-oxides. This could potentially result in the chemical (Atreya et al., 2007), or electrochemical (Delory et al., 2006; Jackson et al., 2010) decomposition of methane. However, these mechanisms remain difficult to reconcile with the observed $\rm H_2O_2$ levels and the absence of increased levels of CO that would also be produced by such electrochemical activity (Lefèvre and Forget, 2009), and consequently other mechanisms have been proposed.

Aeolian activity also produces transient entrainment of sand grains by wind shear, resulting in repeated ballistic collisions and a consequent mineral comminution (Iversen and Rasmussen, 1999). These aeolian driven collisions have been mimicked by tumbling ampules containing mineral grains (Jensen et al., 2014; Merrison et al., 2010; Nørnberg et al., 2014). In particular, Jensen et al. (2014) suggested that the tumbling of crystalline quartz within borosilicate ampules in the presence of ¹³C methane formed \equiv Si $^{-13}$ CH₃ (silicon carbide) and \equiv Si $^{-}$ OH (Silicon hydroxyl) bonds. This was interpreted as methane decomposition to -CH3 and H+ that were bound to the Si• produced by crystal cleavage during the comminution. It was therefore proposed that this mechanically induced comminution of Si can lead to the sequestration of atmospheric methane on Mars (Jensen et al., 2014). This approach was repeated to produce chlorinated methane from methylated Si via the addition of perchlorates and subsequent heating (Bak et al., 2016). However, Jakobsen et al. (2016) demonstrated in further tumbling experiments in quartz rather than borosilicate ampules that this process formed \equiv Si $^{-13}$ CH $_3$ only on ground borosilicate glass, rather than quartz as initially proposed.

Borosilicate glass is of course not a material found on the Martian surface, while quartz has been estimated to be only 1.4% of the crystalline fraction of the Marian regolith (Bish et al., 2013; Smith and Bandfield, 2012). It is therefore currently unknown whether silicate rocks and minerals that are more representative of the Martian surface are capable of methane sequestration via Si-carbide bond formation. The mineralogy of Martian regolith has been constrained using several supporting analytical approaches (Chevrier and Mathé, 2007). Orbital surveys have shown that the primary silicate paragenesis on Mars is mafic basaltic (45-52% SiO₂) to extrusive volcanic andesitic/basaltic (52-63% SiO₂). This has been uniformly distributed globally across the surface and has been grouped according to the differences in their relative proportions of olivine, clinopyroxenes, orthopyroxenes, feldspars (Cousin et al., 2017; Downs, 2015; Ehlmann and Edwards, 2014; Larsen et al., 2000; McSween et al., 1999, McSween, 2002, McSween et al., 2003, 2009; Rampe et al., 2017, 2020). Additionally, high-silica phases such as silicate glasses, zeolites, and opal have also been detected in the Martian terrain (Gellert et al., 2004; McSween et al., 2003,

2004; Poulet et al., 2009; Wyatt and McSween, 2002).

We have therefore carried out a new set of tumbling experiments to test whether more representative silicate rocks (basalt and obsidian) and minerals (feldspar, pyroxene, olivine, zeolite, opal) are capable of sequestering $^{13}\mathrm{C\text{--}labeled}$ methane via the formation of Si-carbide bonds. We used magic-angle spinning nuclear magnetic resonance (MAS NMR) following earlier investigations (Bak et al., 2016; Jakobsen et al., 2016; Jensen et al., 2014). However, a drawback with using MAS NMR spectroscopy for the analysis of natural minerals and glasses has been the presence of paramagnetic species such as transition and rare Earth elements that commonly occur in geological materials. These species result in the broadening of peaks and signal deterioration leading to low signal to noise ratios, "smearing" of NMR intensity into the spinning sidebands and peak broadening, leading to significant decreases in the spectral resolution with the subsequent loss of information (Oldfield et al., 1983: Sheriff and Hartman, 1985). This may confound the interpretation of any structural information from MAS NMR spectra and hypothetically peaks could be broadened to the extent that the peak could be lost in the background noise. Nevertheless, chemical reactions in amorphous, poorly crystalline and crystalline materials along with mixtures of molecules in these materials have previously been investigated using MAS NMR (Kirkpatrick, 2018). Indeed, the same minerals that were used in this study have been successfully analysed with MAS NMR in earlier studies (Fyfe et al., 1983; Graetsch et al., 1994; Johnson and Rossman, 2003; Palke et al., 2011; McCarty et al., 2015; Novikov et al., 2017). Thus, while magnetic susceptibility can affect NMR, the complete loss of signal has not been reported for the minerals used here. However, analyses by attenuated total reflectance-Fourier transform infrared spectroscopy (ATR-FTIR) and X-ray photoelectron spectroscopy (XPS), which are unaffected by paramagnetism were used to support the MAS NMR analysis. Additionally, thermogravimetry-differential scanning calorimetry coupled with quadrupole mass spectrometry was used to determine the water content of the minerals used in this investigation, as mineral included water may also react with Si• (Kita et al., 1982).

2. Methods

2.1. Preparation and tumbling to induce low energy abrasion of mineral and rock samples

The nine geological specimens were obtained from different sources. These were selected to serve as analogues for the rock and minerals that have either previously been detected or speculated to be present on the surface of Mars or used in earlier Si comminution investigations (Table 1). The minerals/rocks were broken into 2-5 cm pieces using a hammer and steel plate, then granulated in a stainless steel Tema ring rock pulveriser (Tema Machinery Ltd., Northhamptonshire. UK), for 7–10 s, then sieved to collect the 250 μ m–500 μ m size material. These samples were repeatedly sonicated in deionised water (18.2 $M\Omega \cdot cm^{-1}$) to remove any residual fine dust from the grain surfaces until the deionised water was visibly clear, then samples were dried at 70 °C for 48 h. Ten grams of the cleaned 250 μm -500 μm mineral grains were loaded into 27.1 mL fused silica quartz glass side-arm ampoules that had been bespoke manufactured. The sidearm ampoules and quartz wool were soaked in a 5% HCl solution, overnight and for 4 h respectively the dried overnight. These were then rinsed $4\times$ with deionised water and $2\times$ with MilliQ water. The ampoules were wrapped in foil and placed in a muffle furnace at 550 °C for 300 min. The butyl stoppers were treated in boiling 1 M NaOH for 1 h, rinsed with 18.2 $M\Omega$ cm⁻¹ water then dried for 16 h at 70 $^{\circ}\text{C},$ and crimp sealed. The sealed ampules were evacuated to \leq 5.0 \times 10⁻² mbar on a vacuum line. 5 mL of ¹³C labeled methane gas (490229-1L-EU, Sigma Aldrich, UK) was then injected into the sealed ampules which (after taking into account the slightly different densities and hence volumes of 10 g of each mineral/rock added) gave final estimated pressures of between 207 and 224 mbar.

The samples were tumbled according to the method adapted from

Table 1

The sources for the rocks and minerals that were used in this investigation included analogues that were: ¹Representative of minerals that have been detected on Mars; ²Minerals that were used in previous investigations and ³Minerals that have been speculated to be present on the surface of Mars.

Mineral/Rock sample	Source	Reference
¹ Basalt	Geology Superstore, tertiary, Isle of Skye	(McSween, 2002)
² Borosilicate glass	2 mm diameter beads, Sigma Aldrich (Product code: Z273627)	(Bak et al., 2016)
¹ Feldspar	Plagioclase Feldspar (Albite-Anorthite) Geology Superstore, Osedalen, Southern Norway	(Larsen et al., 2000)
³ Obsidian	Geology Superstore, Aheim, Western Norway	(Greeley et al., 1982)
¹ Olivine	Forsterite, Geology Superstore,	(Bish et al., 2013; McSween et al., 2004)
¹ Opal	Green Opal mine run rough – Madagascar, Fantasia mining.	(Squyres et al., 2008)
¹ Pyroxene	Augite-pyroxene, 1 kg, cleavages, Wards Science (VWR)	(McSween et al., 2004)
² Quartz (crystalline)	Geology Superstore, Quartz points, Madagascar	(Smith and Bandfield, 2012; Bish et al., 2013)
¹ Zeolite	Natural zeolite (Clinoptilolite), from eBay seller Freyberg (8844).	(Ruff, 2004)

(Jensen et al., 2014), using an adapted MX-RL-Pro LCD Digital Rotisserie Tube Rotator (Scilogex Rocky Hill, CT, USA) to mimic the aeolian driven abrasion on the surface of Mars (See S-1.0). The ampules were tangentially loaded to discs and rotating at 40 rpm (0.67 Hz rotational frequency) for 240 days producing a total of \sim 27.65 \times 10⁶ ampule inversions. The power input to the grains was estimated from the gravitational energy (E) expended as a function of drop length in Earth gravity (Merrison et al., 2010; Merrison, 2012).

$$E = mgh, (1)$$

where:

E = Energy(W)

m = Mass of the mineral grains (kg)

g = Earth gravitational acceleration (m.s⁻¹)

h = Drop height of grains (m).

Here $m = 1.0 \times 10^{-2}$ kg, $g = 1.0 \times 10^{1}$ m·s⁻¹ and $m = 7 \times 10^{-2}$ m. Thus, each inversion generated 7.0×10^{-3} watts of energy, and a total of $1.9 \times 10^7 \, \text{W} \cdot \text{g}^{-1}$ were generated from the ca. 2.8×10^7 inversions. It has previously been estimated that the power transfer threshold from the wind to grains sufficient to generate mobilisation of quartz sand grains is on Earth ca. $7.0 \times 10^{-1} \, \text{W} \cdot \text{kg}^{-1}$ (Iversen and Rasmussen, 1999) and this has been used to crudely estimate the level of saltation that may in Martian gravity (Merrison, 2012) that was equivalent to ca. 5.0×10^{-2} W·kg⁻¹. Using this estimation, tumbling for 240 days generated an energy input equivalent to ca. 3360 days and ca. 9.2 Earth years (ca. 3275 sols and ca. 4.9 Martian years) of continuous quartz mobilisation in the Martian gravity. After tumbling, the material was passed through a 250 μm sieve and the 500–250 μm grains and <250 μm fractions and stored in screw-top glass vials sealed with Al foil. The fraction of the pretumbled material of grain sizes that was comminuted to <250 µm has been presented in supplementary material Table S-2.0. Thermogravimetry-differential scanning calorimetry coupled with quadrupole mass spectrometry was performed to determine the relative proportions of water in the minerals. The method was adapted from Lopez-Capel et al. (2006), using the protocol described in Supplementary Material S-3.1. The m/z 18 ions (H₂O), calorimetry and gravimetry data for each of the minerals were presented in the supplementary information S-3.2. Magnetic susceptibility of the minerals according to their mass (γ_g) was measured using a magnetic susceptibility balance (Sherwood Scientific ltd, Cambridge, UK) using an MnCl standard to calibrate these

measurements. The magnetic susceptibility was calculated based on the mass of each sample.

2.2. Cross-polarisation magic-angle spinning nuclear magnetic resonance spectroscopy

The tumbled grains <250 µm that were prepared according to Section 2.1, alongside borosilicate glass and quartz that had not been tumbled in methane (pre-tumbled), were loaded into a Magic Angle Spinning rotor, then analysis performed using solid-state ¹³C using Cross-Polarisation Magic Angle Spinning Nuclear Magnetic Resonance Spectroscopy (CPMAS NMR). ²⁹Si CPMAS NMR was also performed to see if ²⁹Si peaks were smeared or broadened by paramagnetic effects. Cross-Polarisation Total Suppression of Spinning Sidebands (CPTOSS NMR) analysis was also performed on samples that demonstrated positive Si—¹³C bond formation (borosilicate and the quartz samples). The spectra were recorded at 125.78 MHz using a Bruker Avance III HD 500 spectrometer equipped with a MASSB-DR-BB/1H&19F- 4 mm probe. The spectra were obtained using cross-polarisation with a 4 s recycle delay, 2 ms contact time and 20,480 scans (total acquisition time 22 h, 46 min). Data were recorded at ambient probe temperature (25 °C) and a spin rate of 6 kHz, with an additional 8 kHz analysis performed on the borosilicate and quartz samples to provide a greater definition of the spectral peaks. Spectra referencing was with respect to an external sample of neat tetramethylsilane (performed by setting the highfrequency signal from adamantane to 37.8 ppm).

2.3. Attenuated total reflectance Fourier transform infra-red spectroscopy

The tumbled mineral grains <250 µm that were prepared according to Section 2.1 and pre-tumbled samples were analysed using infra-red spectroscopy. This was conducted in the mid to far-infrared range, using a Nicolet 4100 Fourier transform infra-red (FTIR) spectrometer (Thermo Fisher Scientific, MA, U.S.A.), with a diamond platform attenuated total reflectance (ATR) module (Specac Ltd. London, UK) attached. Background scans were taken before each analytical scan and spectra were obtained from 32 replicate scans conducted between 4000 cm⁻¹ to 550 cm⁻¹, in 4 cm⁻¹ steps. Spectra were analysed using Omnic 8.2.0.387 software (Thermo Fisher Scientific, MA, U.S.A.). Linear background deduction was performed and the spectra between 1400 cm⁻¹ to 550 cm⁻¹ have been presented here. Band identification was conducted using the Sigma Aldrich FTIR table (www.sigmaaldrich. com/technical-documents/articles/biology/ir-spectrum-table.html) and bands derived from standard materials reported in the literature (Kleinová et al., 2015; Reig et al., 2002).

2.4. X-ray photoelectron spectroscopy

A 1 mm deep layer of tumbled grains <250 μ m that were prepared according to Section 2.1 and pre-tumbled material, were immobilised onto SEM stubs using carbon tape then slotted into the XPS analysis plate. This 1 mm deep sample layer was in excess of the 1–10 nm depth of analysis. XPS analysis was conducted using a Thermo Scientific K-alpha X-ray Photoelectron SpectrometerTM (Thermo Scientific, East Grinstead, UK). Survey spectra (broad energy, multiple elements) were used to obtain the quantitative elemental data from the obtained with scans between -5.0 eV and 1350.0 eV; a dwell time of 50 ms; a step size of 1.0 eV and a pass energy of 200.0 eV.

High resolution (narrow scan, single element) carbon 1 s (C1s) and silicon (Si2p) spectra were collected at 40 eV pass energy with a 0.1 eV step size. Spectra were acquired using a monochromatic Al K α X-ray source with an output energy of 1486.6 eV with a maximum X-ray beam spot size of 400 μm . Surface charge compensation was obtained with a low energy dual-beam electron/ion flood gun operated at 40 eV. Spectral analysis was carried out using CasaXPS software (CasaXPS Ltd. Teignmouth, UK) with major peaks selected for element identification

using the Handbook of X-ray photoelectron spectroscopy (Chastain and King, 1995). Any energy shifts were calibrated using the Na1s binding energy at 1072.0 eV. The carbide binding energy was obtained from the La Surface online database (www.lasurface.com) and confirmed with a high-resolution XPS C1s scan of a silicon carbide standard (Product number: 378097, Sigma Aldrich, Dorset, UK), see Supplementary Material S-4.0.

3. Results

3.1. Detection of Si-carbide bonds using total suppression of spinning sideband nuclear magnetic resonance analysis

The NMR analysis confirmed that Si—C (silicon carbide) bonds were formed in borosilicate glass tumbled in the presence of ¹³C methane (Fig. 1b). This was consistent with the observations made in earlier investigations (Bak et al., 2017; Jakobsen et al., 2016; Jensen et al., 2014). Si—C bonds were also detected in the crystalline quartz samples, contrary to Jakobsen et al. (2016). In addition to these silicon carbide bonds, peaks that can be assigned to hydrocarbon and hydroxyl bonds were also present (Table 2) in the borosilicate and quartz samples. The detection of these bonds suggested that mechanochemically induced side reactions with either free or bound O2 potentially took place during the tumbling. In contrast, no ¹³C bonds were detected in borosilicate or quartz glass before tumbling (supplementary material S-5.0) or in any other sample (Fig. 1a, 1c-g, 1h) other than the borosilicate glass and the quartz. NMR analysis could not be conducted on the pyroxene sample (Fig. 1g); despite several attempts, the rotor could not be made to spin stably and so no data could be collected. Analysis of the borosilicate sample using a pulse sequence with no cross-polarisation and a longer relaxation delay (60 s) showed that the Si-C was the dominant carbon environment. The prohibitively long experiment times prevented obtaining quantifiable results (spectra with adequate signal/noise ratio to be able to observe and integrate all the carbon peaks).

The results of the ²⁹Si CPMAS NMR spectra demonstrate that sharp

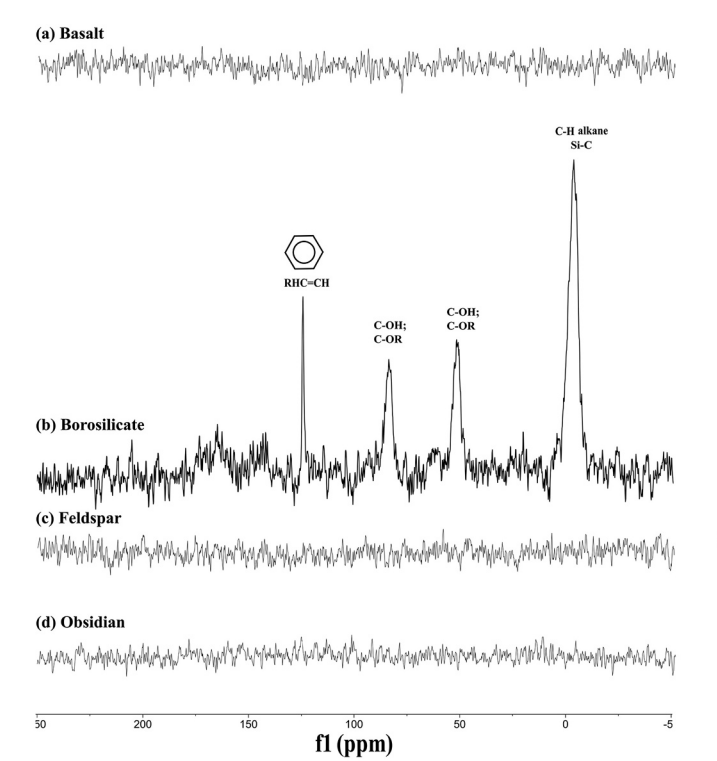


Table 2 The CPMAS NMR chemical shifts produced by the chemical bonds that were associated with the 13 C following tumbling for 240 days (see Fig. 1).

	Chemical shift (ppm)		
Chemistry	Borosilicate	Quartz	
Si— ¹³ C (silicon carbide) ¹³ C—OH/ ¹³ COR, (hydroxyl/carboxyl) 13C—OH/RC=CR ₂ (hydroxyl/alkyne) RH ¹³ C=CH, (aromatic)	-2.5 52 75 130	-3 53 80 125	

peaks for ²⁹Si were still visible for borosilicate glass, quartz, feldspar, opal, zeolite and obsidian, but were completely absent for basalt and olivine (Supplementary Material, S-5.1).

3.2. Attenuated total reflectance-Fourier transform infrared spectroscopy (ATR-FTIR) analysis

Fig. 2a-i presented the ATR-FTIR spectra for the samples used in this investigation. This showed that bands distributed around 780 \pm 20 cm $^{-1}$ were detected in the ATR-FTIR spectra of the quartz (Fig. 2b) and borosilicate (Fig. 2h) samples following tumbling but were not present in the respective pre-tumbled samples. This band was consistent with the presence of Si-C (Kleinová et al., 2015) and implied that Si carbide bond formation occurred in these two samples as a result of tumbling. The 780 \pm 20 cm⁻¹ bands were not detected in the basalt, feldspar, obsidian, olivine, opal, pyroxene and zeolite samples (Figs. 2a, 2c-g and 2i) either before or after tumbling. This indicated that Si-C bond formation did not occur in these samples. This was consistent with the detection of Si carbide bonds in borosilicate and quartz, using CPMAS NMR (Fig. 1b and 1h). Furthermore, the zeolite ATR-FTIR spectra indicated that a band at 765 \pm 20 cm cm $^{-1}$ was present that was bounded by the range where a Si—C band could occur. However, a band at this position is also bounded by absorbance from C-H bending at $755 \pm 20 \text{ cm}^{-1}$ and given that Si carbide bonds were not detected in the

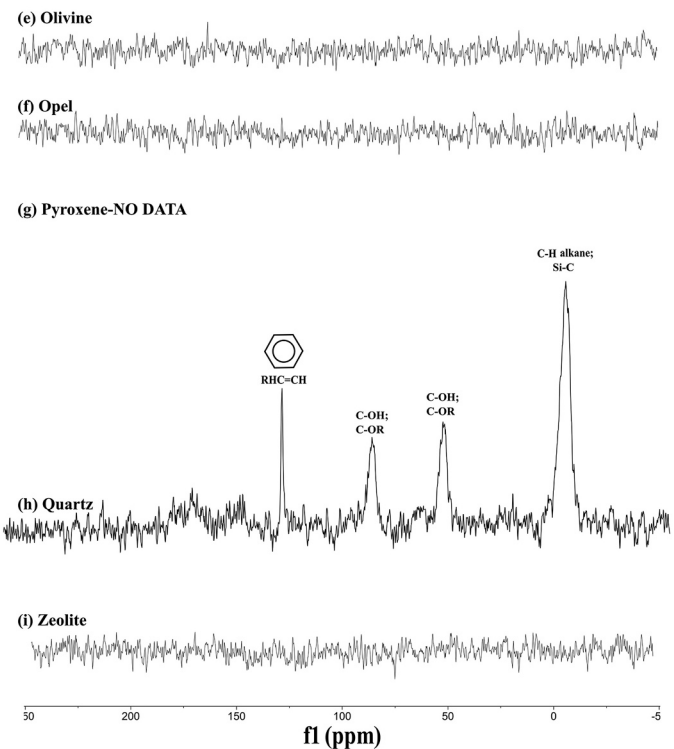


Fig. 1. (a-i): NMR spectra obtained from samples serving as analogues for the Martian geology following tumbling for 240 days. Peaks are annotated with their chemical bond assignments (Table 2).

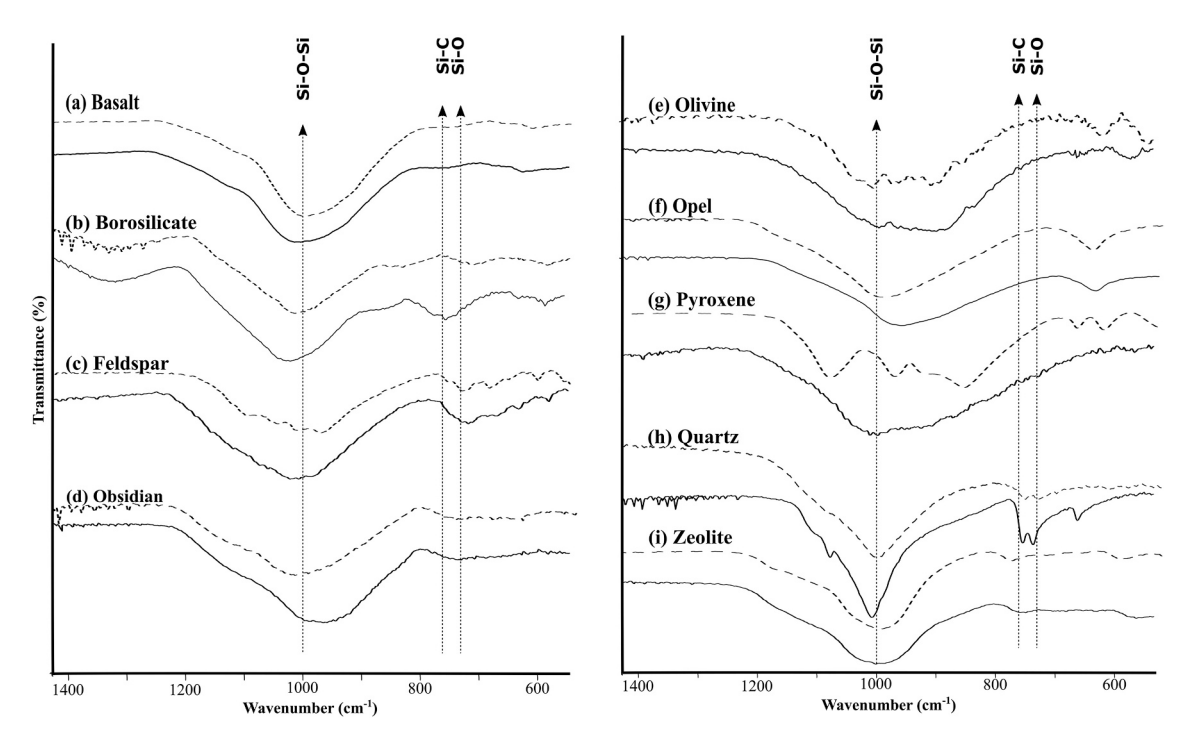


Fig. 2. FTIR spectra between 1400 cm⁻¹ and 550 cm⁻¹ obtained from samples following tumbling serving as analogues for the Martian geology. The peak centred on 1000 cm⁻¹ band is indicative of Si—O—Si bonding and the band distributed around 780 cm⁻¹ were consistent with those assigned to Si—C by Kleinová et al. (2015). Broken lines indicate rock and mineral before tumbling and solid lines after tumbling.

CPMAS NMR (Fig. 1) and XPS spectra (Fig. 2) then this was likely attributable to be due to C—H bending. Therefore, the ATR-FTIR analysis was consistent with carbide bond formation in only the borosilicate and quartz, using CPMAS NMR (Figs. 1b and 1h). No data could be obtained from the CPMAS NMR analysis of the pyroxene samples (Fig. 1g). However, the ATR-FTIR analysis indicated that a band at 780 cm⁻¹ was not present in the pre-tumbled and tumbled pyroxene spectra (Fig. 2g broken and solid lines), which implied carbide bonds did not form in the pyroxene sample due to tumbling.

3.3. X-ray photoelectron spectroscopy (XPS) analysis

The spectral profiles of borosilicate and quartz samples (Figs. 3b and h) spanned the part of the spectrum that included the 282.8 \pm 0.1 eV binding energy, which was consistent with the presence of a C-Si bonding environment (La surface.com), which was confirmed by the peak at 282 eV in the Si carbide standard (S-3). The peaks at the position were not present in the pre-tumbled samples or the other samples used in this investigation (Fig. 3 a-i, broken lines and S-6.1 for synthetic peak fitting). These results permitted a C—Si synthetic component to be fitted at 282.0 eV to the XPS C1s of tumbled borosilicate and quartz (S-6.2). High-resolution XPS C1s scans (Figs. 3a-i) also showed that a range of carbon-carbon and carbon-oxygen chemical states could be detected in all the samples used in this investigation, but XPS could not attribute this to the ^{13}C labeled methane. A $\underline{\text{Si}}\text{---}\text{C}$ component could not be fitted to the high-resolution Si 2p XPS spectra, which was the reciprocal of the C—Si of the high-resolution C1s XPS spectra. This was due to the high surface concentration of Si-O and overlapping synthetic components could be assigned to both the Si-O bonds (binding energy 100.0 eV) and the Si—C bonds (binding energy: 100.4 eV), confounding additional support for the assignment of a C—Si component in the C1s high-resolution spectra. Additionally, the XPS survey (broad) scan was able to quantitatively measure the elemental composition in all the rock and mineral samples.

The XPS survey spectra with the elements that were detected and their relative surface concentrations and are presented in

Supplementary Material S-7.0. The XPS survey spectra showed that basalt, feldspar, obsidian, olivine, opal, pyroxene and zeolite all possessed one or more transition or lanthanide elements. In contrast, these elements were not present in the borosilicate glass or the quartz samples (Table 3).

4. Discussion

Earlier investigations showed that the comminution of Si-rich borosilicate glass, through tumbling in the presence of methane, led to the formation of Si• that became methylated and that such a mechanism might explain the higher than calculated loss of methane from the Martian atmosphere (Jensen et al., 2014; Bak et al., 2016; Jakobsen et al., 2016; Bak et al., 2017). Here we verified that tumbling borosilicate glass in methane resulted in Si carbide bond formation, but, contrary to Jakobsen et al. (2016) Si—¹³C bonds were also detected in quartz. The CP MAS NMR, ATR-FTIR and XPS each produced results that were consistent and mutually supportive. Importantly, this is the first conclusive demonstration that the tumbling of a natural silicate mineral in a Martian analogue atmosphere can result in the drawdown of methane and formation of silica carbide bonds.

The absence of Si—¹³C bonds in our MAS NMR analysis in the remaining Si-rich minerals and rocks (basalt, feldspar, obsidian, olivine opal, and zeolite) following the tumbling in ¹³C methane was unexpected. One potential explanation for this is that Si—¹³C had been formed during the experiments, but their presence in the MAS-NMR spectrum were obscured by the presence of magnetic transition elements. All of the minerals and rock that were used in this investigation, other than the borosilicate glass, quartz and feldspar, were paramagnetic (Table 3). This paramagnetism can result in the "smearing" of NMR intensity into the spinning sidebands and peak broadening (Oldfield et al., 1983; Sheriff and Hartman, 1985; Keating and Knight, 2007) which could in theory lead to MAS NMR peaks being completely subsumed into the background noise. To check for this effect, we also ran ²⁹Si CPMAS NMR spectra to see if ²⁹Si peaks were smeared and broadened in each of the materials. The Cross-Polarisation experiment was

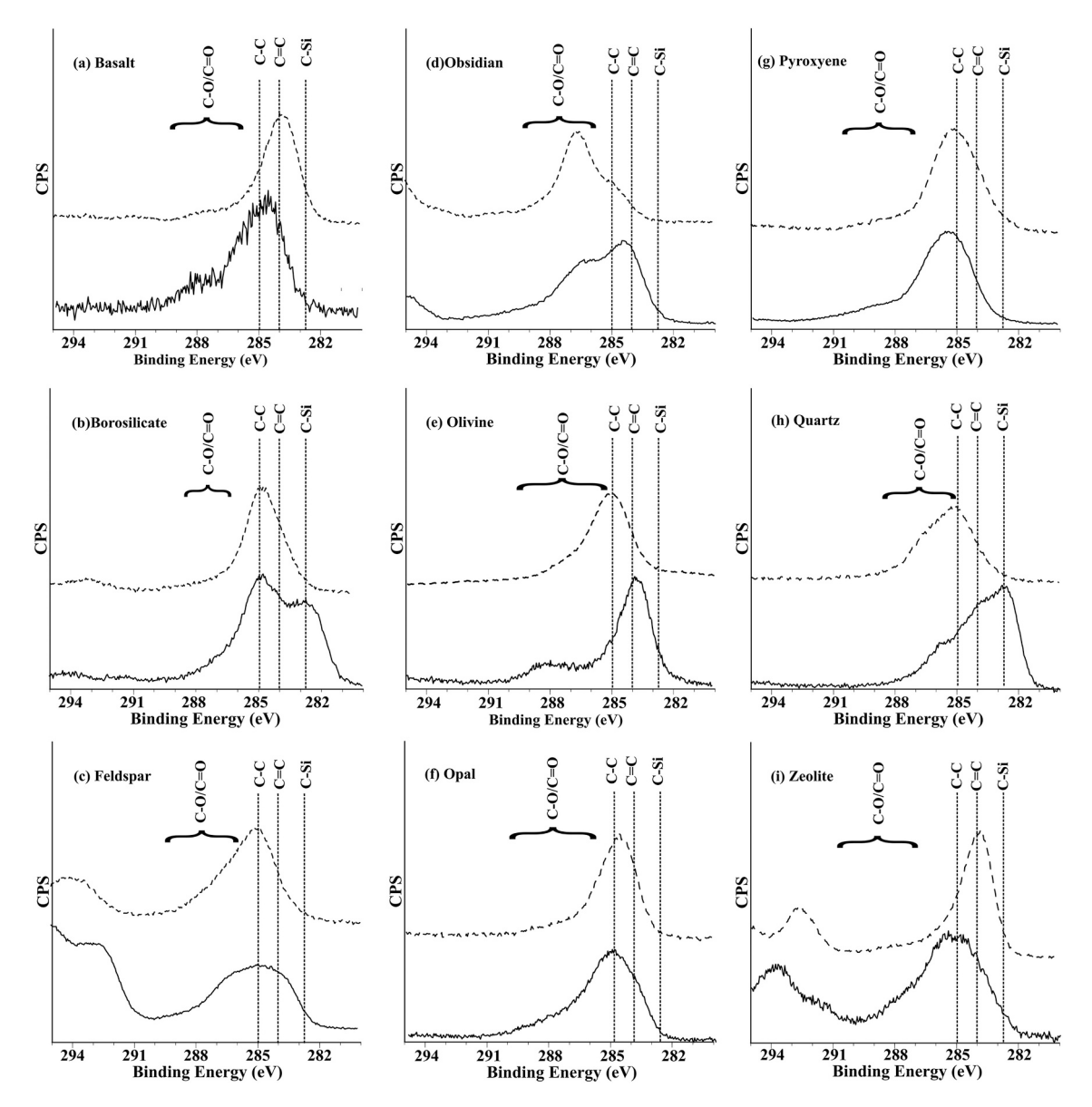


Fig. 3. High-resolution XPS C1s spectra of the samples used in this investigation, comparing the pre-tumbled (broken line) with the samples that were tumbled for 240 days (solid line). The abscissa was an arbitrary scale, CPS = counts per second.

Table 3The rock and mineral samples that were used in this investigation, with their chemical formula and the transition element and lanthanides that were detected by XPS and their magnetic susceptibility by mass.

Rock and mineral sample	Chemical Form##ula	Transition element	Magne suscept 10^{-8})	tic tibility ($\chi_g \times$
Basalt	CaMgSi ₂ O ₆	Fe	1802	Paramagnetic
Borosilicate glass	B ₂ Na ₂ SiO ₈	Not present	-6	Diamagnetic
Feldspar	NaAlSiO ₃	Fe, Cr, Tb	-67	Diamagnetic
Obsidian	MgFe ₃ SiO ₇	Fe, Tb	306	Paramagnetic
Olivine	Mg_2SiO_4	Dy, Pd	138	Paramagnetic
Opal	SiO ₂ ·H ₂ O	Fe, Co, Cr, Y	43	Paramagnetic
Pyroxene	(Fe,Mg)Si ₂ O ₆	Fe, Y, Dy, Tm	184	Paramagnetic
Quartz	SiO_2	Not Present	-6	Diamagnetic
Zeolite	$Na_2Al_2Si_2O_8$	Fe, Y	25	Paramagnetic

used as it was believed to be more representative of the surface chemistry (the experiment depends on nearby protons, which are more likely to be on the surface of the mineral). The results demonstrate that clear

sharp peaks for 29 Si were still visible for borosilicate glass, quartz, feldspar, opal, zeolite and obsidian, but were completely absent for basalt and olivine (S-5.1). This indicates that a) we cannot use the apparent absence of Si $^{-13}$ C peaks in basalt and olivine as a reliable indicator, and, b) the absence of Si $^{-13}$ C peaks in feldspar, opal, zeolite and obsidian is more likely to be indicative of a real absence.

Importantly the XPS and FTIR spectroscopy data used as additional supporting information to test for the presence of Si¹³C are unaffected by paramagnetism. In particular, the shift in binding energy in the C1s spectrum resulting from C—Si bonds has little overlap with the binding energies of any other carbon chemistry, therefore the XPS results should provide a robust test. The XPS results show positive Si¹³C bond formation only in borosilicate glass and quartz (Section 3.3; Fig. 3), corroborating the MAS-NMR results. Similarly, the FTIR results are consistent with Si¹³C formation only in borosilicate glass and quartz (Section 3.2; Fig. 2). We therefore conclude that the absence of Si¹³C formation in our suite of Mars analogue samples (basalt, feldspar, obsidian, olivine opal, and zeolite) is real. We further suggest the absence of Si—C was not due to limitations in the sensitivity of the three instruments used in this investigation. The rock and the minerals were tumbled in the presence of

pure methane gas at a pressure of 207 to 224 mbar; i.e. a $>10^7 \times$ greater concentrations than the 15.5 ppbv methane spike measured in the Martian atmosphere (Webster et al., 2015; Giuranna et al., 2019). Si—C bond formation occurs on the surfaces during crystal cleavage. Therefore, the Si• and any Si—C bonds that formed through comminution would be concentrated on the surfaces of the samples. XPS is sensitive to the chemistry concentrated on the top 1–10 nm of the sample surfaces and this confirmed that <u>C</u>—Si bonds formed exclusively on the borosilicate and quartz samples.

The reasons for the lack of methane uptake by basalt, feldspar, obsidian, olivine, opal, and zeolite are uncertain. The TGA analysis of the samples (S-3.2) indicated that there was no association between water in the samples and Si-C formation. This suggested that Si reacting with water did not suppress Si-C formation. However, the XPS survey (broad scan) spectra unambiguously showed that, in addition to the known elemental constituents of basalt, feldspar, obsidian, olivine, opal, and zeolite, these samples also contained one or more transition elements as contaminants. Importantly, these were not present in the borosilicate glass and quartz samples (Table 3 and S-7.0). We hypothesise that one or more of these transition elements could have donated an e⁻ to the Si•, which suppressed the formation of the Si—C bonds. The Martian regolith is characteristically dominated by Fe and possesses other redox-active (multiple oxidation state) transition elements. Fe²⁺ minerals, such as magnetite, appear to be present below the surface (Goetz et al., 2007; Christensen et al., 2008; Rampe et al., 2020), which could serve as e donors. We further suggest that the differences seen for tumbled quartz in our study where Si-C bonds were detected (Figs. 1h, 2h and 3h, S-6.2) compared to earlier investigations where they were not (Jakobsen et al., 2016) might be explained by differences in the redox-active element composition of the different quartzes. However, the source and composition for the quartz in Jakobsen et al. (2016) were not reported and further experiments will be needed to test this hypothesis.

Crystalline quartz comprises only an estimated 1.4% of the crystalline fraction of the regolith on Mars (Bish et al., 2013; Smith and Bandfield, 2012). Consequently, our results imply that wind-driven methane sequestration via Si—C bond formation may only occur to an extremely limited extent and may therefore be unlikely to have a significant impact on the rates of destruction of Martian atmospheric methane. Consequently, we suggest that other process(es) such as dust devils and dust storms which may result in electrochemical reactions (Delory et al., 2006; Jackson et al., 2010), the production of superoxides that become embedded on the regolith that are capable of decomposing organic material (Atreya et al., 2006) or triboelectrical reactions (Atreya et al., 2007) may be more likely as candidate mechanisms for rapid methane decomposition in the Martian atmosphere.

In addition to the Si—13C that were formed on the comminuted borosilicate glass and quartz samples, the NMR results also detected ¹³Clabeled hydrocarbon and hydroxyl chemistry (Fig. 1b and h; Table 2). This is consistent with mechanochemically driven addition reactions also occurring during the slower tumbled comminution of both the borosilicate glass and quartz during the 240-day investigation here. The induction of further addition reactions through the tumbling of quartz is consistent with prior reports of mechanochemically driven polymerization reactions during the high energy comminution of quartz (Hasegawa et al., 2001). The oxygen required for the formation of hydroxyl bonds may have been derived from either the dissociation of any traces of free O2 remaining during the experimental set-up or from the dissociation of the traces of water within the minerals (See S-3.2). However, crystalline quartz is uncommon on Mars, hence any aeolian driven polymerization reactions would not be expected to have a significant impact on Martian geochemistry.

5. Conclusion

A combination of MAS NMR, ATR-FTIR and XPS have confirmed

prior reports that the tumbling of borosilicate glass in a methane atmosphere, mimicking the aeolian-driven saltation of sand grains, can sequester methane in the form of solid-phase silica-carbide (Si-C) bonds. We have further demonstrated that the tumbling of quartz can also form the same Si-C bonds. It was anticipated that comparable carbide bonds would also form on a variety of other silicate-rich minerals/rocks (basalt, feldspar, opal, olivine, zeolite) more representative of the surface geology on Mars. However, no Si-C bonds were detected in any of these samples. The reason or reasons for this is unclear. We observed a correlation between the presence of redox-active transition elements, including Fe, and the absence of Si-C formation. We speculated that the redox-active elements may donate an electron to the Si• that form through comminution which suppresses the formation of the Si—C bonds. Our results indicate that the minerals typically found on the surface of Mars will not promote significant Si-C formation during aeolian abrasion and therefore aeolian driven saltation of the Martian regolith appears to be an unlikely mechanism for the higher-thanexpected loss of methane from the Martian atmosphere. Therefore, other mechanisms are probably responsible for an efficient methane sink on Mars and these require investigation.

Data availability

All raw data is available for this study is available for public access at https://doi.org/10.25405/data.ncl.17104559.v1.

Declaration of Competing Interest

No competing financial interests or other competing interests exist.

Acknowledgments

The authors wish to thank Onoriode Esegbue for conducting the thermogravimetric analysis of the samples and acknowledge financial support from UK Space Agency Aurora grants ST/R001421/1 and ST/S001484/1 (to J.T.). We thank to UK Engineering and Physical Sciences Research Council (EPSRC), on grant number NS/A000015/1 for support for NEXUS facility.

Appendix A. Supplementary data

Supplementary data to this article can be found online at https://doi.org/10.1016/j.icarus.2021.114827.

References

- Atreya, S.K., Wong, A.S., Renno, N.O., Farrell, W.M., Delory, G.T., Sentman, D.D., Cummer, S.A., Marshall, J.R., Rafkin, S.C.R., Catling, D.C., 2006. Oxidant enhancement in martian dust devils and storms: implications for life and habitability. Astrobiology. 6 (3), 439–450.
- Atreya, S.K., Mahaffy, P.R., Wong, A.S., 2007. Methane and related trace species on Mars: origin, loss, implications for life, and habitability. Planet. Space Sci. 55 (3), 358–369.
- Bak, E.N., Jensen, S.J.K., Nornberg, P., Finster, K., 2016. Methylated silicates may explain the release of chlorinated methane from Martian soil. Earth Planet. Sci. Lett. 433, 226–231.
- Bak, E.N., Zafirov, K., Merrison, J.P., Jensen, S.J.K., Nørnberg, P., Gunnlaugsson, H.P., Finster, K., 2017. Production of reactive oxygen species from abraded silicates. Implications for the reactivity of the Martian soil. Earth Planet. Sci. Lett. 473, 113–121.
- Bish, D.L., Blake, D.F., Vaniman, D.T., Chipera, S.J., Morris, R.V., Ming, D.W., Treiman, A.H., Sarrazin, P., Morrison, S.M., Downs, R.T., Achilles, C.N., Yen, A.S., Bristow, T.F., Crisp, J.A., Morookian, J.M., Farmer, J.D., Rampe, E.B., Stolper, E.M., Spanovich, N., 2013. X-ray diffraction results from mars science laboratory: mineralogy of rocknest at Gale crater. Science, 341 (6153).
- Chastain, J., King, R.C. (Eds.), 1995. Handbook of X-Ray Photoelectron Spectroscopy: A Reference Book of Standard Spectra for Identification and Interpretation of XPS Data. Physical Electronics. Eden Prairie. MN.
- Chevrier, V., Mathé, P.E., 2007. Mineralogy and evolution of the surface of Mars: a review. Planet. Space Sci. 55 (3), 289–314.
- Christensen, P.R., Bandfield, J.L., Rogers, A.D., Glotch, T.D., Hamilton, V.E., Ruff, S.W., Wyatt, M.B., 2008. Global mineralogy mapped from the Mars global surveyor

- thermal emission spectrometer. In: The Martian Surface-Composition, Mineralogy, and Physical Properties ${\bf p.195}.$
- Cousin, A., Sautter, V., Payré, V., Forni, O., Mangold, N., Gasnault, O., Le Deit, L., Johnson, J., Maurice, S., Salvatore, M., Wiens, R.C., Gasda, P., Rapin, W., 2017. Classification of igneous rocks analyzed by ChemCam at Gale crater, Mars. *Icarus*. 288, 265–283.
- Delory, G.T., Farrell, W.M., Atreya, S.K., Renno, N.O., Wong, A.S., Cummer, S.A., Sentman, D.D., Marshall, J.R., Rafkin, S.C.R., Catling, D.C., 2006. Oxidant enhancement in Martian dust devils and storms: storm electric fields and electron dissociative attachment. Astrobiology. 6 (3), 451–462.
- Downs, R.T., 2015. Determining mineralogy on Mars with the CheMin X-ray diffractometer. Elements. 11 (1), 45–50.
- Ehlmann, B.L., Edwards, C.S., 2014. Mineralogy of the Martian surface. Annu. Rev. Earth Planet. Sci. 42.
- Formisano, V., Atreya, S., Encrenaz, T., Ignatiev, N., Giuranna, M., 2004. Detection of methane in the atmosphere of Mars. Science. 306 (5702), 1758–1761.
- Franz, H.B., Mahaffy, P.R., Webster, C.R., Flesch, G.J., Raaen, E., Freissinet, C., Atreya, S. K., House, C.H., McAdam, A.C., Knudson, C.A., Archer, P.D., Stern, J.C., Steele, A., Sutter, B., Eigenbrode, J.L., Glavin, D.P., Lewis, J.M.T., Malespin, C.A., Millan, M., et al., 2020. Indigenous and exogenous organics and surface-atmosphere cycling inferred from carbon and oxygen isotopes at Gale crater. Nat. Astron. 4 (5), 526–532.
- Fyfe, C.A., Thomas, J.M., Klinowski, J., Gobbi, G.C., 1983. Magic-angle-spinning NMR (MAS-NMR) spectroscopy and the structure of zeolites. Angew. Chem. Int. Ed. Eng. 22 (4), 259–275.
- Gellert, R., Reider, R., Anderson, R.C., Brückner, J., Clark, B.C., Dreibus, G., Economou, T., Klingelhôfer, G., Lugmair, G.W., Ming, D.W., Squyres, S.W., D'Uston, C., Wänke, H., Yen, A., Zipfel, J., 2004. Chemistry of rocks and soils in Gusev crater from the alpha particle x-ray spectrometer. Science. 305 (5685), 829–832.
- Giuranna, M., Viscardy, S., Daerden, F., Neary, L., Etiope, G., Oehler, D., Formisano, V., Aronica, A., Wolkenberg, P., Aoki, S., Cardesín-Moinelo, A., Marín-Yaseli de la Parra, J., Merritt, D., Amoroso, M., 2019. Independent confirmation of a methane spike on Mars and a source region east of Gale Crater. Nat. Geosci. 12 (5), 326–332.
- Goetz, W., Madsen, M.B., Hviid, S.F., Gellert, R., Gunnlaugsson, H.P., Kinch, K.M., Klingelhöfer, G., Leer, K., Olsen, M., 2007. The nature of Martian airborne dust. Indication of long-lasting dry periods on the surface of Mars. In: Seventh International Conference on Mars, Vol. 1353, p. 3104.
- Graetsch, H., Gies, H., Topalović, I., 1994. NMR, XRD and IR study on microcrystalline opals. Phys. Chem. Miner. 21 (3), 166–175.
- Greeley, R., Leach, R.N., Williams, S.H., White, B.R., Pollack, J.B., Krinsley, D.H., Marshall, J.R., 1982. Rate of wind abrasion on Mars. J. Geophys. Res. Solid Earth 87 (B12), 10009–10024.
- Hasegawa, M., Kimata, M., Kobayashi, S.I., 2001. Mechanochemical polymerization of styrene initiated by the grinding of quartz. J. Appl. Polym. Sci. 82 (11), 2849–2855.
- Iversen, J.D., Rasmussen, K.R., 1999. The effect of wind speed and bed slope on sand transport. Sedimentology. 46 (4), 723–731.
- Jackson, T.L., Farrell, W.M., Delory, G.T., Nithianandam, J., 2010. Martian dust devil electron avalanche process and associated electrochemistry. J. Geophys. Res. E. Planets. 115 (E5).
- Jakobsen, H.J., Song, L., Gan, Z., Hung, I., Bildsøe, H., Skibsted, J., Bak, E.N., Finster, K., Nørnberg, P., Knak Jensen, S.J., 2016. NMR and EPR studies of free-radical intermediates from experiments mimicking the winds on mars: a sink for methane and other gases. J. Phys. Chem. C 120 (45), 26138–26149.
- Jensen, S.J.K., Skibsted, J., Jakobsen, H.J., ten Kate, I.L., Guimlaugsson, H.P., Merrison, J.P., Finster, K., Bak, E., Iversen, J.J., Kondrup, J.C., Nornberg, P., 2014. A sink for methane on Mars? The answer is blowing in the wind. Icarus 23624–23627.
- Johnson, E.A., Rossman, G.R., 2003. The concentration and speciation of hydrogen in feldspars using FTIR and 1H MAS NMR spectroscopy. Am. Mineral. 88 (5–6), 901–911
- Keating, K., Knight, R., 2007. A laboratory study to determine the effect of iron oxides on proton NMR measurements. Geophysics 72 (1), E27–E32.
- Kirkpatrick, R.J., 2018. MAS NMR spectroscopy of minerals and glasses. Spectr. Methods Mineral. Geol. 341–404.
- Kita, I., Matsuo, S., Wakita, H., 1982. H₂ generation by reaction between H₂O and crushed rock: an experimental study on H₂ degassing from the active fault zone. J. Geophys. Res. Solid Earth 87 (B13), 10789–10795.
- Kleinová, A., Huran, J., Sasinková, V., Perný, M., Šály, V., Packa, J., 2015. FTIR spectroscopy of silicon carbide thin films prepared by PECVD technology for solar cell application. In: Reliability of Photovoltaic Cells, Modules, Components, and Systems VIII [Online]. 2015 p.
- Korablev, O., Vandaele, A.C., Montmessin, F., Fedorova, A.A., Trokhimovskiy, A., Forget, F., Lefevre, F., Daerden, F., Thomas, I.R., Trompet, L., Erwin, J.T., Aoki, S., Robert, S., Neary, L., Viscardy, S., Grigoriev, A.V., Ignatiev, N.I., Shakun, A., Patrakeev, A., et al., 2019. No detection of methane on Mars from early ExoMars trace gas orbiter observations. Nature. 568 (7753), 517–520.
- Krasnopolsky, V.A., Maillard, J.P., Owen, T.C., 2004. Detection of methane in the martian atmosphere: evidence for life? Icarus. 172 (2), 537–547.
- Larsen, K.W., Arvidson, R.E., Jolliff, B.L., Clark, B.C., 2000. Correspondence and least squares analyses of soil and rock compositions for the Viking Lander 1 and Pathfinder landing sites. J. Geophys. Res. E Planets. 105 (E12), 29207–29221.
- Lefèvre, F., Cavalazzi, B., Westall, F., 2019. The enigma of methane on Mars. In:
 Biosignatures for astrobiology, 1st edition. Springer, Berlin Heidelberg, pp. 253–266
 [Online].
- Lefevre, F., Forget, F., 2009. Observed variations of methane on Mars unexplained by known atmospheric chemistry and physics. Nature. 460 (7256), 720–723.

Lopez-Capel, E., Abbott, G.D., Thomas, K.M., Manning, D.A.C., 2006. Coupling of thermal analysis with quadrupole mass spectrometry and isotope ratio mass spectrometry for simultaneous determination of evolved gases and their carbon isotopic composition. J. Anal. Appl. Pyrolysis 75 (2), 82–89.

- McCarty, R.J., Palke, A.C., Stebbins, J.F., Hartman, J.S., 2015. Transition metal cation site preferences in forsterite (Mg₂SiO₄) determined from paramagnetically shifted NMR resonances. Am. Mineral. 100 (5–6), 1265–1276.
- McSween, H.Y., 2002. The rocks of Mars, from far and near. Meteorit. Planet. Sci. 37 (1), 7–25.
- McSween, H.Y., Murchie, S.L., Crisp, J.A., Bridges, N.T., Anderson, R.C., Bell, J.F., Britt, D.T., Brückner, J., Dreibus, G., Economou, T., Ghosh, A., Golombek, M.P., Greenwood, J.P., Johnson, J.R., Moore, H.J., Morris, R.V., Parker, T.J., Rieder, R., Singer, R., et al., 1999. Chemical, multispectral, and textural constraints on the composition and origin of rocks at the Mars pathfinder landing site. J. Geophys. Res. E Planets. 104 (E4), 8679–8715.
- McSween, H.Y., Grove, T.L., Wyatt, M.B., 2003. Constraints on the composition and petrogenesis of the Martian crust. J. Geophys. Res. E Planets. 108 (E12).
- McSween, H.Y., Arvidson, R.E., Bell, J.F., Blaney, D., Cabrol, N.A., Christensen, P.R., Clark, B.C., Crisp, J.A., Crumpler, L.S., Des Marias, D.J., Farmer, J.D., Gellert, R., Ghosh, A., Gorevan, S., Graff, T., Grant, J., Haskin, L.A., Herkenhoff, K.E., Johnson, J.R., et al., 2004. Basaltic rocks analyzed by the Spirit rover in Gusev crater. Science. 305 (5685), 842–845.
- McSween, H.Y., Jeffrey Taylor, G., Wyatt, M.B., 2009. Elemental composition of the martian crust. Science. 324 (5928), 736–739.
- Merrison, J.P., 2012. Sand transport, erosion and granular electrification. Aeolian Res. 4, 1-16.
- Merrison, J.P., Gunnlaugsson, H.P., Jensen, S.K., Nornberg, P., 2010. Mineral alteration induced by sand transport: a source for the reddish color of martian dust. Icarus. 205 (2), 716–718.
- Moores, J.E., Gough, R.V., Martinez, G.M., Meslin, P.Y., Smith, C.L., Atreya, S.K., Mahaffy, P.R., Newman, C.E., Webster, C.R., 2019. Methane seasonal cycle at gale crater on Mars consistent with regolith adsorption and diffusion. Nat. Geosci. 12 (5), 321–325.
- Mumma, M.J., Villanueva, G.L., Novak, R.E., Hewagama, T., Bonev, B.P., DiSanti, M.A., Mandell, A.M., Smith, M.D., 2009. Strong release of methane on Mars in northern summer 2003. Science. 323 (5917), 1041–1045.
- Nørnberg, P., Bak, E., Finster, K., Gunnlaugsson, H.P., Iversen, J.J., Jensen, S.K., Merrison, J.P., 2014. Aeolian comminution experiments revealing surprising sandball mineral aggregates. Aeolian Res. 13, 77–80.
- Novikov, A.N., Neuville, D.R., Hennet, L., Gueguen, Y., Thiaudière, D., Charpentier, T., Florian, P., 2017. Al and Sr environment in tectosilicate glasses and melts: viscosity, Raman and NMR investigation. Chem. Geol. 461, 115–127.
- Oehler, D.Z., Etiope, G., 2017. Methane seepage on mars: where to look and why. Astrobiology 17 (12), 1233–1264.
- Oldfield, E., Kinsey, R.A., Smith, K.A., Nichols, J.A., Kirkpatrick, R.J., 1983. High-resolution NMR of inorganic solids. Influence of magnetic centers on magic-angle sample-spinning lineshapes in some natural aluminosilicate. J. Magn. Reson. 51 (2), 325–329
- Palke, A., Stebbins, J.F., Frost, D.J., McCammon, C.A., 2011, December. 27 Al and 29 Si NMR spectroscopy of MgSiO3 perovskite: mechanisms of Al and Fe incorporation. In: AGU Fall Meeting Abstracts, Vol. 2011 (pp. MR31A-2194).
- Poulet, F., Mangold, N., Platevoet, B., Bardintzeff, J.M., Sautter, V., Mustard, J.F., Bibring, J.P., Pinet, P., Langevin, Y., Gondet, B., Aléon-Toppani, A., 2009. Quantitative compositional analysis of martian mafic regions using the MEx/OMEGA reflectance data. 2. Petrological implications. Icarus. 201 (1), 84–101.
- Rampe, E.B., Ming, D.W., Blake, D.F., Bristow, T.F., Chipera, S.J., Grotzinger, J.P., Morris, R.V., Morrison, S.M., Vaniman, D.T., Yen, A.S., Achilles, C.N., 2017. Mineralogy of an ancient lacustrine mudstone succession from the Murray formation, Gale crater, Mars. Earth Planet. Sci. Lett. 471, 172–185.
- Rampe, E.B., Blake, D.F., Bristow, T.F., Ming, D.W., Vaniman, D.T., Morris, R.V., Achilles, C.N., Chipera, S.J., Morrison, S.M., Tu, V.M., Yen, A.S., 2020. Mineralogy and geochemistry of sedimentary rocks and eolian sediments in Gale crater, Mars: a review after six Earth years of exploration with Curiosity. Geochemistry 80 (2) (p.125605).
- Reig, F.B., Adelantado, J.V.G., Moreno, M.C.M.M., 2002. FTIR quantitative analysis of calcium carbonate (calcite) and silica (quartz) mixtures using the constant ratio method. Application to geological samples. Talanta. 58 (4), 811–821.
- Ruff, S.W., 2004. Spectral evidence for zeolite in the dust on Mars. Icarus. 168 (1), 131-143.
- Seto, M., Noguchi, K., Van Cappellen, P., 2019. Potential for aerobic methanotrophic metabolism on mars. Astrobiology. 19 (10), 1187–1195.
- Sheriff, B.L., Hartman, J.S., 1985. Solid-state high-resolution 29 Si NMR of feldspars; Al-Si disorder and the effects of paramagnetic centres. Canad. Mineral. 23 (2), 205–212.
 Smith, M.R., Bandfield, L.J. 2012. Geology of quarty and bydrated silica-hearing.
- Smith, M.R., Bandfield, J.L., 2012. Geology of quartz and hydrated silica-bearing deposits near Antoniadi crater, Mars. J. Geophys. Res. Planets 117 (E6).
- Squyres, S.W., Arvidson, R.E., Ruff, S., Gellert, R., Morris, R.V., Ming, D.W., Crumpler, L., Farmer, J.D., Des Marais, D.J., Yen, A., McLennan, S.M., Calvin, W., Bell, J.F., Clark, B.C., Wang, A., Mccoy, T.J., Schmidt, M.E., de Souza, P.A., 2008. Detection of silica-rich deposits on Mars. Science. 320 (5879), 1063–1067.
- Summers, M.E., Lieb, B.J., Chapman, E., Yung, Y.L., 2002. Atmospheric biomarkers of subsurface life on Mars. Geophys. Res. Lett. 29 (24).
- Webster, C.R., Mahaffy, P.R., Atreya, S.K., Flesch, G.J., Farley, K.A., 2013. Low upper limit to methane abundance on Mars. Science. 342 (6156), 355–357.
- Webster, C.R., Mahaffy, P.R., Atreya, S.K., Flesch, G.J., Mischna, M.A., Meslin, P.Y., Farley, K.A., Conrad, P.G., Christensen, L.E., Pavlov, A.A., Martin-Torres, J., Zorzano, M.P., McConnochie, T.H., Owen, T., Eigenbrode, J.L., Glavin, D.P.,

Steele, A., Malespin, C.A., Archer, P.D., et al., 2015. Mars methane detection and

- variability at Gale crater. Science. 347 (6220), 415–417.

 Webster, C.R., Mahaffy, P.R., Atreya, S.K., Moores, J.E., Flesch, G.J., Malespin, C., McKay, C.P., Martinez, G., Smith, C.L., Martin-Torres, J., Gomez-Elvira, J., Zorzano, M.P., Wong, M.H., Trainer, M.G., Steele, A., Archer, D., Sutter, B., Coll, P.J., Freissinet, C., et al., 2018. Background levels of methane in Mars' atmosphere show strong seasonal variations. Science. 360 (6393), 1093-1096.
- Wong, A.S., Atreya, S.K., Encrenaz, T., 2003. Chemical markers of possible hot spots on Mars. J. Geophys. Res. Planets 108 (E4).
- Wyatt, M.B., McSween, H.Y., 2002. Spectral evidence for weathered basalt as an alternative to andesite in the northern lowlands of Mars. Nature. 417 (6886), 263-266.